Available online at www.sciencedirect.com
SCIENCE DIRECT
Journal of Power Sources 155 (2006) 190–202
JOURNAL OF POWER SOURCES
www.elsevier.com/locate/jpowsour

Water and pressure effects on a single PEM fuel cell

Biao Zhou *, Wenbo Huang, Yi Zong, Andrzej Sobiesiak

Department of Mechanical, Automotive and Materials Engineering, University of Windsor, Ont., Canada N9B 3P4

Received 1 March 2005; accepted 2 April 2005
Available online 20 June 2005

Abstract

A fuel cell is a promising energy conversion system that will eventually become the first-choice for producing power because of its clean or zero-emission nature. A steady-state, two-dimensional mathematical model with pressure and phase change effects for a single PEM fuel cell was developed to illustrate the inlet humidification and pressure effects on proton exchange membrane (PEM) fuel cell performance. This model considers the transport of species along the channel as well as water transfer through the membrane. It can be used to predict trends of the following parameters along the fuel cell channels: mole number of liquid water and water vapor, pressure, temperature, density, viscosity, velocity, saturation pressure, pressure drop, vapor mole fraction, volume flow rate, required pumping power and current density.

Keywords: PEM fuel cell; Water and thermal management; Mathematical model; Humidification; Pressure drop

1. Introduction

Proton exchange membrane (PEM) fuel cells, using hydrogen as fuel, emitting water and operating at low temperature for quick startup, have been widely recognized as the most promising candidates for replacing the internal combustion engine in automobiles, and for replacing batteries in portable and micro applications. In recent years, research and development on fuel cells have accelerated and the PEM fuel cell technology has been successfully demonstrated. But many key challenges affecting PEM fuel cell performance still exist, and much more efforts on improving the performance of PEM fuel cell become even more crucial than ever before. Useful mathematical models can provide powerful tools for the analysis and optimization of fuel cell performance.

Costamagna and Srinivasan [1] gave a very good review regarding fuel cell science and technology up to the year 2000. Another recent review made by Yao et al. [2] presented both empirical performance models and theoretical models. In the early 1990s, the pioneering work on PEM fuel cell model development was done by Bernardi and Verbrugge [3,4], and Springer et al. [5] who formulated one-dimensional and isothermal models for the gas-diffusion layer, active catalyst layer and ion-exchange membrane. Only the direction perpendicular to the membrane was considered. The model employed water diffusion coefficient, electro-osmotic drag coefficients and membrane conductivities to predict the change of membrane resistance with current density. The temperature was assumed to be constant and these models were unable to simulate the flow behavior along the channels.

Compared with one-dimensional model, a two-dimensional mathematical model is preferred for water and heat management analysis, as the temperature, pressure and water varies along the channel as well as across the membrane. Fuller and Newman [6] developed a non-isothermal model by including material balances in the channel, concentration and temperature gradients along the channel as well as across the membrane surface. In the model developed by Nguyen and White [7], the focus was on the transport and reaction in the MEA and heat balances in the gas channels. Subsequently, an improved model was developed by Yi and Nguyen [8] to compare different fuel

* Corresponding author. Tel.: +1 519 253 3000x2630; fax: +1 519 973 7007.
E-mail address: bzhou@uwindsor.ca (B. Zhou).

0378-7753/$ – see front matter © 2005 Published by Elsevier B.V.
doi:10.1016/j.jpowsour.2005.04.027

Nomenclature

a	water vapor activity in stream
A_{cross}	the cross-section area of channel (cm^2)
A_{stack}	the heat transfer area in a control volume (cm^2)
c_{MW}	concentration of water at interface of the membrane ($mol\,cm^{-3}$)
$C_{p,i}$	heat capacity of species i ($J\,mol^{-1}\,k^{-1}$)
d	channel height (cm)
D	hydraulic diameter of channel (cm)
D°	a parameter used in the expression for diffusion coefficient of water ($cm^2\,s^{-1}$)
D_{MW}	diffusion coefficient of water ($cm^2\,s^{-1}$)
$f(x)$	friction factor
F	Faraday constant, 96487 C equivalent^{-1}
h	channel width (cm)
I	current (A)
$I(x)$	current density ($A\,cm^{-2}$)
I°	exchange current density for the oxygen reaction ($A\,cm^{-2}$)
k_c	condensation rate constant (s^{-1})
k_p	hydraulic permeability of water in the membrane (cm^2)
L	length of channel (cm)
M_i	molecular weight of species i ($g\,mol^{-1}$)
$M_{m,dry}$	equivalent weight of a dry membrane ($g\,mol^{-1}$)
n_d	electro-osmotic drag coefficient
n_e	the mole number of electrons needed per second for 1 A of current ($mol\,s^{-1}\,A^{-1}$)
N	mole number of species in the stream ($mol\,s^{-1}$)
NE	number of electrons ($A^{-1}\,s^{-1}$)
N_{ch}	number of channel (s)
p	local pressure (Pa)
p_i	partial pressure of species i (Pa)
dp	pressure drop (Pa)
P_{pump}	pumping power (W)
Q	volume flowrate ($m^3\,s^{-1}$)
Re	Reynolds number
R_u	universal ideal gas constant ($8.3144\,J\,mol^{-1}\,K^{-1}$)
RH	relative humidity
T	temperature of stream (K)
T_s	temperature of stack (K)
U	overall heat-transfer coefficient ($J\,s^{-1}\,cm^{-2}\,^{\circ}C^{-1}$)
V	flow velocity ($m\,s^{-1}$)
V_{cell}	cell voltage (V)
x	direction along the channel length
y	direction normal to the channel length

Greek letters

α	excess coefficient
α_{area}	reaction area coefficient
β_{O_2}	mole fraction of oxygen in air (20.9%)
β_{H_2}	mole fraction of hydrogen
η	overpotential for the oxygen reaction (V)
μ	dynamic viscosity ($N\,s\,m^{-2}$)
ρ	density ($kg\,m^{-3}$)
$\rho_{m,dry}$	density of a dry membrane ($g\,cm^{-3}$)
ϕ	water content in stream
σ_m	membrane conductivity ($\Omega^{-1}\,cm^{-1}$)

Subscripts

1A	per ampere
air	dry air
avg	average
A	anode
C	cathode
cell	single fuel cell
concentration	concentration of species in the streams
drag	electro-osmotic drag
e	electron
H_2	hydrogen
H_2O	produced water
in	inlet of channel
MW	water in membrane
N_2	nitrogen
O_2	oxygen
oc	open circuit
pressure	partial pressure in streams
pump	pump
s	stack
sat	saturation
vapor	water vapor
liquid	liquid water
water	all water including vapor and liquid
#	cathode or anode

cell designs with coflow and counterflow heat exchangers. A number of researchers have been conducting fuel cell modeling for many years and made very impressive progress on single cell modeling [9–15]. These models emphasized important characteristics of the membrane and electrode as well as a detailed description of the water content in the membrane. To the authors' knowledge, most of those models assume that there is no temperature and pressure drop along the channel. Most results reported were at high and constant stack temperature (e.g. 90–100 °C), high and constant pressure (e.g. 3 atm) and without considering phase-change effects. But in practical engineering, the PEM fuel cell is usually operated at varying low temperature (e.g. 65–75 °C) and varying low pressure (e.g. about 1.3 atm for 1 kW portable applications), with water phase-change inside the fuel cell flow channels.

In order to meet these challenges, in the present study, a steady-state, two-dimensional mathematical model with pressure effects, water phase-change effects and detailed

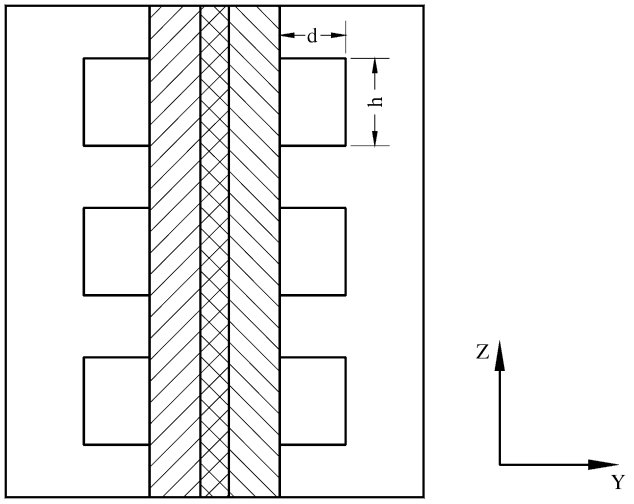

Fig. 1. Schematic diagram of PEM fuel cell modeling regions (*x*-direction: perpendicular to the paper).

mass and heat transfer in a single PEM fuel cell was developed, and the water and pressure effects on a single PEM fuel cell performance were investigated in details.

2. Description of the model

A typical sandwich construction of a PEM fuel cell is shown in Fig. 1. The model regions consist of a proton exchange membrane, two catalyst layers and electrodes at cathode and anode, and two plates with flow channels. The *x*-axis (normal to the paper in Fig. 1) is parallel to the gas channels. The temperature, pressure and concentration of gas flow will be predicted along this direction. The *y*-axis is normal to the membrane. The hydrogen ions and some water molecules transport from anode to cathode along this *y*-direction. At the anode, humidified hydrogen gas is supplied at a given excess coefficient into the flow anode channels. Hydrogen gas diffuses through the porous electrode and reaches the anode catalyst layer, then the chemical reaction, $2H_2 \rightarrow 4H^+ + 4e^-$, releases electrons and creates hydrogen ions which pass through the membrane and reach the cathode. At the cathode, humidified air or pure oxygen with a given excess coefficient flows along the cathode channels, then diffuses through the electrode layer and meets with hydrogen ions, the reaction, $O_2 + 4e^- + 4H^+ \rightarrow 2H_2O$, occurs. Water vapor is produced along the cathode channels and at the same time electrical energy and heat are released.

2.1. Basic assumptions

In the present model, the following assumptions were employed:

(1) Only water vapor can diffuse into electrode and pass through the membrane.
(2) The electrode layer is "ultra thin", therefore gas diffusion through the porous electrode layer is neglected.
(3) The gases and water vapor are treated as being well mixed, the mixture is assumed to be an ideal gas.
(4) Water is produced in the electrochemical reaction in vapor form.
(5) Liquid water is assumed to exist in the form of small droplets and its volume is negligible.
(6) No voltage drop along the flow channels is assumed.
(7) The channels in the single cell are in the same condition.
(8) The solid phase temperatures are the same and constant.

2.2. Mass balance

The amount of inlet gases is calculated according to the electro-chemical reaction for a PEM fuel cell, $2H_2 + O_2 = 2H_2O + 4e^-$. One equivalence of electrons is 1 mole of electrons or 6.022×10^{23} electrons (Avagadro's number). The charge on one mole of electrons is 96,487 coulombs (C) (Faraday's constant). Thus, the charge of a single electron is 1.602×10^{-19} C. One ampere of current is defined as $1\,C\,s^{-1}$. Therefore, the mole number of electrons needed per second for 1 A of current is as follows:

$$n_e = \frac{NE_{1\,A}}{6.022 \times 10^{23}} = 1.03656546 \times 10^{-5}\,\text{mole}\,A^{-1}\,s^{-1} \quad (1)$$

where $NE_{1\,A}$ represents the number of electrons for 1 A and can be calculated by $NE_{1\,A} = 1/1.602 \times 10^{-19}$. Based on the reaction equation, the theoretical mole numbers of consumed oxygen and hydrogen, and produced water for 1 A current output can be obtained by the following equations:

$$n_{O_2,1\,A} = \tfrac{1}{4} n_e \quad (2)$$

$$n_{H_2O,1\,A} = \tfrac{1}{2} n_e \quad (3)$$

$$n_{H_2,1A} = \tfrac{1}{2} n_e \quad (4)$$

The excess coefficients for air (oxygen) or hydrogen is defined as:

$$\alpha = \frac{\text{actually supplied mole number of air (oxygen) or hydrogen}}{\text{theoretically consumed mole number of air (oxygen) or hydrogen}} \quad (5)$$

Therefore, the supplied oxygen, nitrogen and hydrogen mole numbers for 1 A current output can be calculated by the following equations:

$$n_{O_2,in,1\,A} = \alpha_{O_2} n_{O_2,1\,A} \quad (6)$$

$$n_{N_2,in,1\,A} = n_{O_2,in,1\,A} \times \frac{1 - \beta_{O_2}}{\beta_{O_2}} \quad (7)$$

$$n_{H_2,in,1\,A} = \frac{\alpha_{H_2} n_{H_2,1\,A}}{\beta_{H_2}} \quad (8)$$

where β_{O_2} is the mole fraction of oxygen in air ($\beta_{O_2} = 20.9\%$) and β_{H_2} is the mole fraction of hydrogen in anode ($\beta_{H_2} = 1$ in the present study).

For generating I amperes current, the molar flow rates of oxygen, nitrogen and hydrogen for the single channel are therefore evaluated as (mol s^{-1}):

$$N_{C,O_2,in} = I \times \frac{n_{O_2,in,1\,A}}{N_{ch}} \tag{9}$$

$$N_{C,N_2,in} = N_{C,O_2,in} \times \frac{1-\beta_{O_2}}{\beta_{O_2}} \tag{10}$$

$$N_{A,H_2,in} = I \times \frac{n_{H_2,in,1\,A}}{N_{ch}} \tag{11}$$

The components of mixture vary along the gas channels and the local molar flow rates in channel are evaluated as follows:

$$\frac{dN_{C,O_2}(x)}{dx} = -n_{O_2,1\,A} \times I(x) \times h \times \alpha_{area} \tag{12}$$

$$\frac{dN_{C,N_2}(x)}{dx} = 0 \tag{13}$$

$$\frac{dN_{A,H_2}(x)}{dx} = -n_{H_2,1\,A} \times I(x) \times h \times \alpha_{area} \tag{14}$$

where α_{area} is the reaction area coefficient that accounts for the land area for reaction due to gas diffusion from the channel to diffusion layer.

The variation of vapor and liquid water along the channels is more complicated. Vapor water transport and condensation and liquid water evaporation are considered in this model. Three water transport mechanisms across the membrane, according to Yi and Nguyen [8], are considered (a) electro-osmotic drag: since hydrogen ions pass through the membrane, the water molecules are carried from the anode to the cathode; (b) back-diffusion by the concentration gradient of water: because the water concentration is different, some water molecules diffuse from the cathode to the anode; (c) convection by the pressure gradient: water moves from higher-vapor-pressure side to the lower one. The water flux due to electro-osmotic drag in y-direction is evaluated as [7]:

$$N_{drag}(y) = \frac{n_d(x) I(x)}{F} \tag{15}$$

where $I(x)$ is the local current density of the fuel cell, F the Faraday's constant and n_d is the electro-osmotic drag coefficient representing the number of water molecules carried by a single proton calculated by [7]:

$$n_d(x) = \begin{cases} 0.0049 + 2.02a(x) - 4.53a^2(x) + 4.09a^3(x), & 0 < a(x) \le 1 \\ 1.5849 + 0.159(a(x) - 1), & a(x) > 1 \end{cases} \tag{16}$$

where $a(x)$ is the activity of water vapor in membrane. Since the membrane is placed between cathode and anode, the water vapor activity in the membrane is affected by the water vapor activity in the flows at both cathode and anode. A weighted average water activity for water vapor activity in membrane is employed. The water vapor activity at anode or cathode, $a_{\#}(x)$, is defined similar to that in Reference [7], while the pressure $p_{\#}(x)$ is a variable, not a constant as in Reference [7].

$$a_{\#}(x) = \frac{N_{\#,vapor}(x)}{\sum_i N_{\#,i}(x)} \times \frac{p_{\#}(x)}{p_{\#,sat}(x)} \quad (i,\ \text{the species in the flow stream \#}) \tag{17}$$

The diffusion flux caused by concentration gradient of water can be written as follows:

$$N_{concentration}(y) = D_{MW}\left(\frac{\partial c_{MW}}{\partial y}\right) \tag{18}$$

where the diffusion coefficient of water is evaluated as [7]:

$$D_{MW} = \begin{cases} (0.0049 + 2.02a(x) - 4.53a^2(x) + 4.09a^3(x))D^{\circ} \exp\left[2416\left(\frac{1}{303} - \frac{1}{T_s(x)}\right)\right], & \text{for } 0 < a(x) \le 1 \\ 1.59 + 0.159[(a(x) - 1)]D^{\circ} \exp\left[2416\left(\frac{1}{303} - \frac{1}{T_s(x)}\right)\right], & \text{for } a(x) > 1 \end{cases} \tag{19}$$

Convection flux caused by pressure gradient can be evaluated in a similar way to that in Reference [8]. The difference is that the pressure drop along the channel is considered in the present study while it was neglected in Reference [8].

$$N_{pressure}(y) = \left[\frac{c_{MW,C}(x) + c_{MW,A}(x)}{2}\right] \times \frac{k_P}{\mu_W(x)} \times \left(\frac{\partial p_{\#,vapor}(x)}{\partial y}\right) \tag{20}$$

where $p_{\#,vapor}$ is the water vapor pressure in the anode or cathode channels, k_p the permeability of water in the membrane, $\mu_W(x)$ the water viscosity and $c_{MW,C}(x)$ and $c_{MW,A}(x)$ are the concentrations of water in cathode and anode, respectively,

and are expressed as [7]:

$$c_{\mathrm{MW},\#}(x) = \begin{cases} \dfrac{\rho_{\mathrm{m,dry}}}{M_{\mathrm{m,dry}}}[0.043 + 17.8a_{\#}(x) - 39.8a_{\#}^2(x) + 36.0a_{\#}^3(x)], & \text{for } 0 < a_{\#}(x) \le 1 \\ \dfrac{\rho_{\mathrm{m,dry}}}{M_{\mathrm{m,dry}}}[14 + 1.4(a_{\#}(x) - 1)], & \text{for } a_{\#}(x) > 1 \end{cases} \quad (21)$$

$\rho_{\mathrm{m,dry}}$ and $M_{\mathrm{m,dry}}$ are the density and the equivalent weight of a dry proton exchange membrane.

Therefore, the change of water flux along the channel at the cathode can be expressed by:

$$\frac{\mathrm{d}N_{\mathrm{C,water}}(x)}{\mathrm{d}x} = [n_{\mathrm{H_2O}} \times I(x) + N_{\mathrm{drag}}(y) - N_{\mathrm{concenatration}}(y) - N_{\mathrm{pressure}}(y)] \times h\alpha_{\mathrm{area}} \quad (22)$$

The water flux variation along the channel in anode can be expressed by:

$$\frac{\mathrm{d}N_{\mathrm{A,water}}(x)}{\mathrm{d}x} = [-N_{\mathrm{drag}}(y) + N_{\mathrm{concenatration}}(y) + N_{\mathrm{pressure}}(y)] \times h\alpha_{\mathrm{area}} \quad (23)$$

The mole number of water condensation or evaporation can be calculated in a similar way to that in Reference [7], while in the present study, the pressure is different at different location x (pressure was constant in Reference [7]):

$$\frac{\mathrm{d}N_{\#,\mathrm{liquid}}(x)}{\mathrm{d}x} = \left(\frac{k_{\mathrm{c}}hd}{R_{\mathrm{u}}T_{\#}(x)}\right)\left[\frac{N_{\#,\mathrm{vapor}}(x)}{\sum_i N_{\#,i}(x)} \times p_{\#}(x) - p_{\#,\mathrm{sat}}(x)\right] \quad (i,\ \text{the gaseous species in stream \#}) \quad (24)$$

2.3. Energy balance

Based on the assumption that the temperature of solid phase is constant, the latent heat and the heat transfer to mixture flows from solid phase are considered in the present study. The temperatures of the mixture flows can be calculated as [7],

$$\sum_i [N_{\#,i}(x)C_{p,i}(x)]\frac{\mathrm{d}T_{\#}(x)}{\mathrm{d}x} = [H_{W,\mathrm{vapor}}(x) - H_{\mathrm{W,liquid}}(x)]\frac{\mathrm{d}N_{\#,\mathrm{liquid}}(x)}{\mathrm{d}x} + U_{\#}h(T_{\mathrm{s}} - T_{\#}(x)) \quad (i,\ \text{the species in the flow stream \#}) \quad (25)$$

where

$$H_{\#,\mathrm{vapor}}(x) - H_{\#,\mathrm{liquid}}(x) = 45070 - 41.9[T_{\#}(x) - 273] + 3.44 \times 10^{-3}[T_{\#}(x) - 273]^2 + 2.54 \times 10^{-6}[T_{\#}(x) - 273]^3 - 8.98 \times 10^{-10}[T_{\#}(x) - 273]^4 \quad (26)$$

$U_{\#}$ represents the heat transfer coefficient between the flow stream # and stack.

2.4. Pressure drop

To the authors' knowledge, the pressure drop of mixture gas in the fuel cell flow channels was rarely considered in currently available fuel cell research publications. But in industrial design, it is one of the most important parameters simply because it directly affects the efficiency of a fuel cell system and is directly related to the selection of the system pump.

The saturation pressure (Pa) can be expressed in terms of the local temperature [5]:

$$p_{\mathrm{sat}}(x) = 1.013 \times 10^5 \times 10^{-2.1794+0.02953[T_{\#}(x)-273]-9.1837\times10^{-5}[T_{\#}(x)-173]^2+1.4454\times10^{-7}[T_{\#}(x)-273]^3} \quad (27)$$

Based on the assumption that the mixture is an ideal gas, local volumetric flow ($\mathrm{m^3\,s^{-1}}$) in cathode and anode can be calculated by ideal-gas law.

$$Q_{\#}(x) = \sum_i N_{\#,i}(x) \times R_{\mathrm{u}} \times \frac{T_{\#}(x)}{p_{\#}(x)} \quad (i,\ \text{the gaseous species in stream \#}) \quad (28)$$

Local velocity ($\mathrm{m\,s^{-1}}$) in cathode and anode can be calculated as follows:

$$V_{\#}(x) = \frac{Q_{\#}(x)}{A_{\#,\mathrm{cross}}} \quad (29)$$

where $A_{\#,\mathrm{cross}}$ is the cross-section area of the channel in stream #.

Since the mole fraction of gases in the channel varies, local density ($\mathrm{kg\,m^{-3}}$) also varies due to different components in the flow. It can be calculated by:

$$\rho_{\#}(x) = \sum_i \left[\frac{N_{\#,i}(x)}{\sum_i N_{\#,i}(x)} \times \frac{M_{\#,i}}{1000}\right] \times \frac{p_{\#}(x)}{T_{\#}(x) \times R_{\mathrm{u}}} \quad (i,\ \text{the gaseous species in stream \#}) \quad (30)$$

Local dynamic viscosity can be calculated by interpolation. $\mu_{i,100}$ is the gas dynamic viscosity at 100 °C and $\mu_{i,0}$ is the gas dynamic viscosity at 0 °C. The temperature scope of flow in the calculated cases is 0–100 °C, so, the local dynamic viscosity is

$$\mu_{\#}(x) = \sum_i \left\{ \frac{N_{\#,i}(x)}{\sum_i N_{\#,i}(x)} \times \left[\frac{T_{\#}(x) - 273}{100 - 0} \times (\mu_{i,100} - \mu_{i,0}) + \mu_{i,0} \right] \right\} \quad (i,\ \text{the gaseous species in stream \#}) \tag{31}$$

For laminar flow, pressure drop in each control volume can be expressed as (Pa):

$$\frac{\mathrm{d}p_{\#}(x)}{\mathrm{d}x} = \rho_{\#}(x) \times f_{\#}(x) \frac{V_{\#}^2(x)}{2D} \tag{32}$$

where $f_{\#}(x)$ is the friction factor and D is the hydraulic diameter of the channel. In the present study, the channels are assumed to be straight, thus only friction loss is considered. The local pressure is calculated by the pressure at inlet subtracting the pressure drop from the inlet to current control volume.

$$p_{\#}(x) = p_{\#,\mathrm{in}} - \int_0^x \left[\frac{\mathrm{d}p_{\#}(x)}{\mathrm{d}x} \right] \mathrm{d}x \tag{33}$$

Local required pumping power (W) is:

$$\mathrm{d}P_{\#,\mathrm{pump}}(x) = Q_{\#}(x) \times \mathrm{d}p_{\#}(x) \tag{34}$$

Therefore, total required pumping power (W) in stream # used by the designer to choose a proper pump to maintain the flow can be given by:

$$P_{\#,\mathrm{pump}} = N_{\mathrm{ch}} \times \int_0^L \left[\frac{\mathrm{d}p_{\#}(x)}{\mathrm{d}x} Q_{\#}(x) \right] \mathrm{d}x \tag{35}$$

2.5. Cell potential

The cell potential is expressed as [7]:

$$V_{\mathrm{cell}} = V_{\mathrm{oc}} - \eta(x) - \frac{I(x) t_{\mathrm{m}}}{\sigma_{\mathrm{m}}(x)} \tag{36}$$

where V_{oc} is the open circuit potential of fuel cell and $\eta(x)$ is the cell activation over potential and is calculated as,

$$\eta(x) = \frac{R_{\mathrm{u}} T_{\mathrm{s}}(x)}{0.5F} \ln \left(\frac{I(x)}{I^{\circ} \circ p_{\mathrm{C,O_2}}(x)} \right) \tag{37}$$

where I° is the exchange current density at one atmosphere of oxygen and $p_{\mathrm{C,O_2}}$ is the local partial pressure of oxygen at cathode. It is affected by local pressure, which is not constant in the present study. $\sigma_{\mathrm{m}}(x)$ is the membrane conductivity and calculated by the following equation according to [7]:

$$\sigma_{\mathrm{m}}(x) = [0.00514 \times \frac{M_{\mathrm{m,dry}}}{\rho_{\mathrm{m,dry}}} c_{\mathrm{MW}}(x) - 0.00326] \times \exp \left[1268 \times \left(\frac{1}{303} - \frac{1}{T_{\mathrm{s}}(x)} \right) \right] \tag{38}$$

where

$$c_{\mathrm{MW}}(x) = \begin{cases} \dfrac{\rho_{\mathrm{m,dry}}}{M_{\mathrm{m,dry}}} [0.043 + 17.8a(x) - 39.85a^2(x) + 36.0a^3(x)], & \text{for } 0 < a(x) \le 1 \\ \dfrac{\rho_{\mathrm{m,dry}}}{M_{\mathrm{m,dry}}} [14 + 1.4(a(x) - 1)], & \text{for } a(x) > 1 \end{cases} \tag{39}$$

The average current density is

$$I_{\mathrm{avg}} = \frac{1}{L} \int_0^L I(x)\, \mathrm{d}x \tag{40}$$

3. Solution procedure

The model equations are solved by numerical method at a given value of average current density, I_{avg}. The channel is subdivided into n control volumes of equal length $\Delta L = L/n$ in x-direction. The exit values at the kth control volume are the inlet values at the $(k+1)$th control volume. A set of differential equations is replaced by algebraic equations based on the finite difference method. Based on the given value of I_{avg}, the flow rates for hydrogen, air, water vapor and liquid are calculated. Next, the guessed value for the cell voltage, guessed exit temperatures of flow streams and guessed exit pressure of the kth control volume are chosen. The model equations are solved to get a set of current densities and a new $I_{\mathrm{avg.}}$ If the new I_{avg} is not equal to the given I_{avg}, a new cell voltage is chosen and a new iteration begins until the relative error between the calculated I_{avg} and the given I_{avg} meet the convergence criteria, e.g., 0.001. Inside the iterations, Newton–Raphson method [16] is used to solve the non-linear equations.

4. Results and discussions

For convenience of discussion, a new parameter called relative water content is defined as follows:

$$\phi_{\#}(x) = \frac{\text{mole number of water (vapor + liquid)}}{\text{mole number of water in saturation}} \quad \text{or}$$

$$\phi_{\#}(x) = \frac{N_{\#,\mathrm{water}}(x)}{\sum_i N_{\#,i}(x)} \times \frac{p_{\#}(x)}{p_{\#,\mathrm{sat}}(x)} \quad (i,\ \text{the gaseous species in stream \#}) \tag{41}$$

Table 1
Size of channels and parameter values of electrode and membrane

Parameter	Value
Channel number of cathode and anode (N_{ch})	4
Channel length (L)	83.5 cm
Channel height at anode (d)	0.1 cm
Channel width at anode (h)	0.1 cm
Condensation rate constant (k_c)	1.0 s^{-1}
Dry membrane density ($\rho_{m,dry}$)	2.0 g cm^{-3}
Dry membrane equivalent weight ($M_{m,dry}$)	1100 g mol^{-1}
Membrane thickness (t_m)	0.01275 cm
Diffusion coefficient of water in membrane (D°)	5.5×10^{-7} cm^2 s^{-1}
Water permeability	1.58×10^{-14} cm
Water viscosity	3.565×10^{-3} g $cm^{-1}s^{-1}$
Fuel cell open-circuit voltage (V_{oc})	1.1 V
Current density (I_{avg})	1.0 A cm^{-2}
Oxygen exchange current density (I°)	0.01 A cm^{-2}
Heat-transfer coefficient (U)	0.0025 W cm^{-2} $^\circ C^{-1}$

Calculations were performed for various inlet relative water contents on anode and cathode side, respectively. Pure oxygen or air is supplied into cathode channels. Channels are in rectangular shape and the size of the channel is listed in Table 1. The parameters for the base case are shown in Table 2.

Fig. 2 shows the effect of anode inlet water content on the membrane conductivity. For the same cathode inlet water content, the membrane conductivity increases with the anode inlet water content especially near the inlet, because higher anode inlet water leads to well-hydrated membrane. In anode channel, the liquid water will evaporate to generate water vapor. Fig. 3 shows the effect of cathode inlet water content on the membrane conductivity. It has some effect on the membrane conductivity near the inlet. This effect decreases along the channel because the vapor pressure increases along the cathode channel, and condensation occurs when the vapor pressure is over the saturation pressure.

Fig. 4 shows the local current density profiles with various anode inlet relative water contents when cathode inlet water content is fixed at 1.0. At the front part of the channels, the membrane is well hydrated, which leads to high membrane conductivity and high local current density. The water content of anode side dominates the membrane performance. Therefore, the current density increases with anode

Table 2
Parameter values for the base case

Parameter	Value
Inlet temperature of flow at cathode and anode	333 K
Inlet temperature of solid phase	333 K
Inlet relative water content at anode	0.5, 0.75, 1.0, 1.25
Inlet relative water content at cathode	0.5, 0.75, 1.0, 1.25
Inlet pressure at anode and cathode	1.1×10^5 Pa
Excess coefficient of flow at cathode	2.0
Excess coefficient of flow at anode	2.0

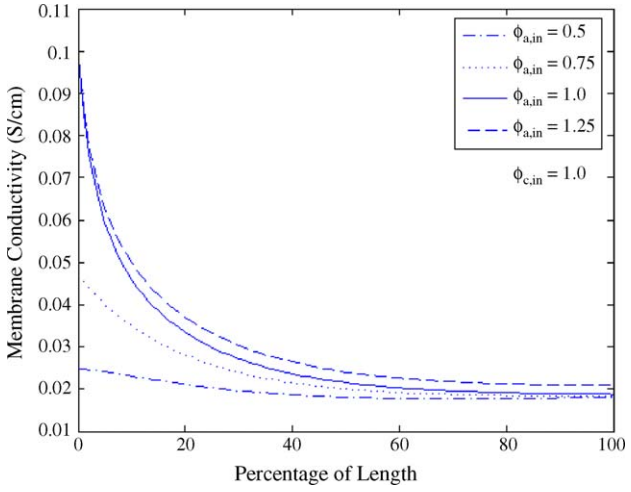

Fig. 2. Effect of anode inlet water content on the membrane conductivity (pure oxygen; $\phi_{c,in} = 1.0$; $\phi_{a,in} = 0.5, 0.75, 1.0, 1.25$).

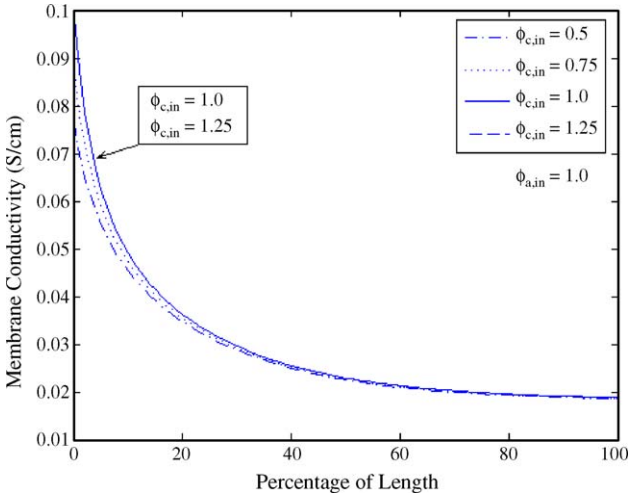

Fig. 3. Effect of cathode inlet water content on the membrane conductivity (pure oxygen; $\phi_{a,in} = 1.0$; $\phi_{c,in} = 0.5, 0.75, 1.0, 1.25$).

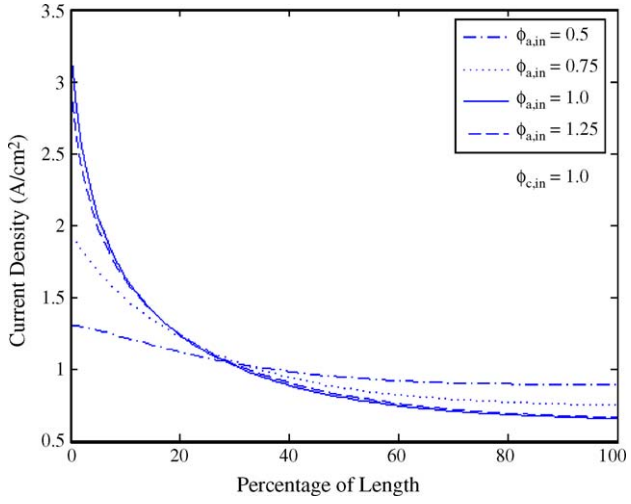

Fig. 4. Effect of anode inlet water content on the current density (pure oxygen; $\phi_{c,in} = 1.0$; $\phi_{a,in} = 0.5, 0.75, 1.0, 1.25$).

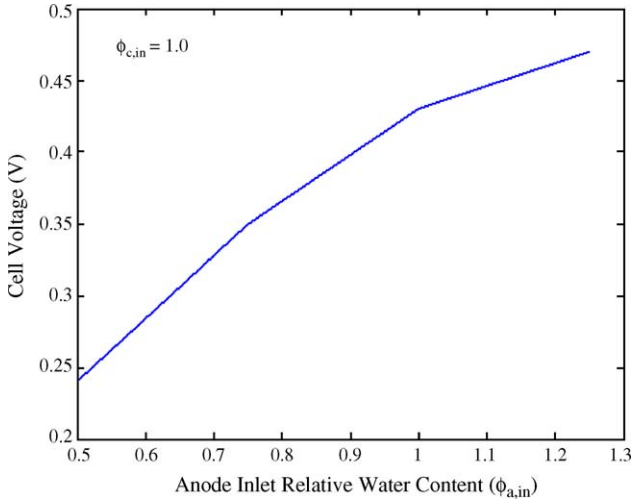

Fig. 5. Effect of anode inlet water content on the cell voltage (pure oxygen).

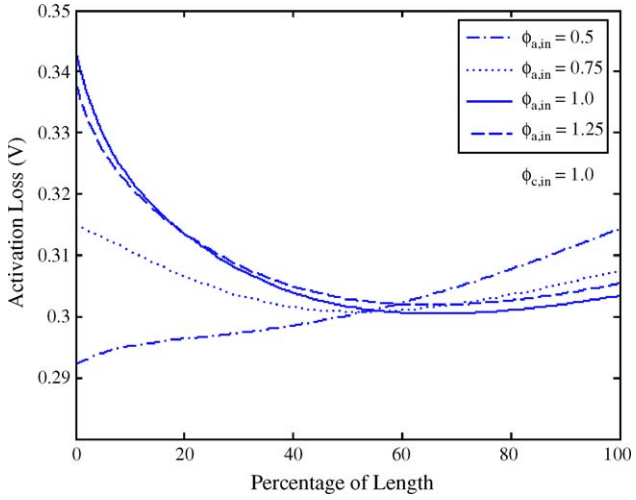

Fig. 7. Effect of anode inlet water content on the activation loss (pure oxygen; $\phi_{c,in}$ = 1.0; $\phi_{a,in}$ = 0.5, 0.75, 1.0, 1.25).

inlet relative water content near the inlet up to the inlet with saturation condition. In Fig. 4, comparing the two cases of $\phi_{a,in}$ = 1.0 and $\phi_{a,in}$ = 1.25, it can be found that if liquid water is supplied ($\phi_{a,in}$ = 1.25), the current density is slightly lower near the inlet. This is because the change of membrane conductivity due to the liquid water ($\phi_{a,in}$ = 1.25) is very small near the inlet (Fig. 2), while the cell voltage for $\phi_{a,in}$ = 1.25 is higher than that of saturation condition ($\phi_{a,in}$ = 1.0) at inlet (Fig. 5). In the downstream channel, the membrane conductivity is better because of the evaporation of liquid water, so the current density is slightly higher than that with saturation condition at inlet. If the anode inlet water content is maintained at 1.0, the effect of cathode inlet water on the local current density is very limited (Fig. 6). This is because membrane performance and water transport are mainly controlled by the water content of anode side.

Fig. 7 shows the anode inlet water effect on the activation loss. In the front part of the channel, the activation loss increases with anode inlet water up to saturation, which agrees with the local current density discussed in Fig. 4. In the rear part of the channel, the effect is reversed due to the combined effects of local current density and partial pressure of oxygen. From Fig. 8, it can be seen that the activation loss increases with the increase of the cathode inlet water content. This is because higher inlet water in cathode leads to lower partial pressure of oxygen. The cathode inlet liquid water has no effect on the activation loss, because the liquid water has no chance to evaporate in this case, since the water vapor in the cathode is always saturated or over-saturated due to the inlet condition with liquid water and water production in cathode.

Figs. 9 and 10 show the effects of anode and cathode inlet water contents on the ohmic loss. The inlet water contents of both sides have similar effect on ohmic loss, i.e., increased amount of inlet water leads to lower ohmic loss. This is because the increased amount of inlet water leads to

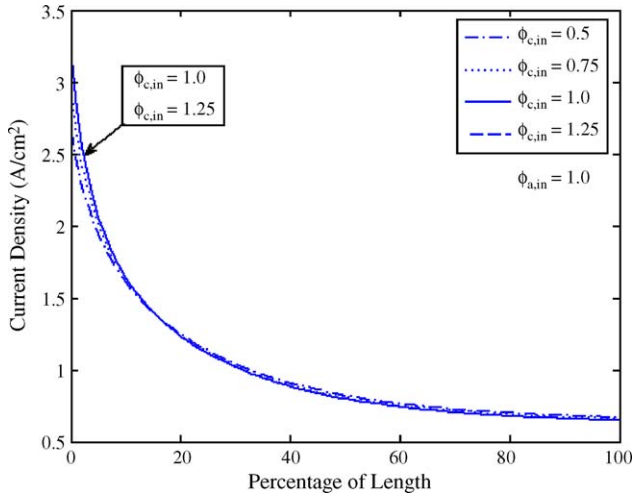

Fig. 6. Effect of cathode inlet water content on the current density (pure oxygen; $\phi_{a,in}$ = 1.0; $\phi_{c,in}$ = 0.5, 0.75, 1.0, 1.25).

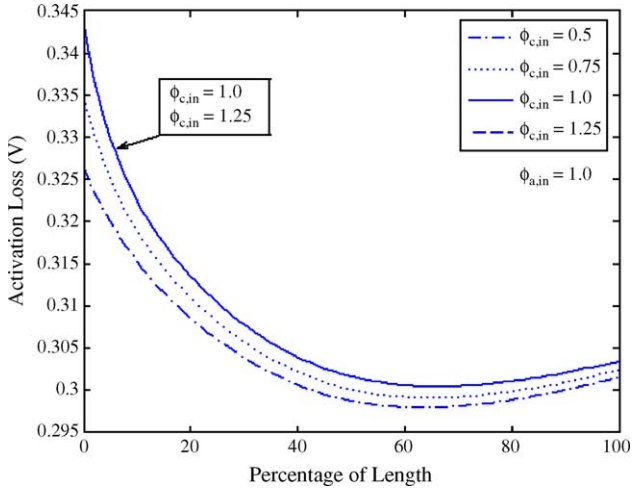

Fig. 8. Effect of cathode inlet water content on the activation loss (pure oxygen; $\phi_{a,in}$ = 1.0; $\phi_{c,in}$ = 0.5, 0.75, 1.0, 1.25).

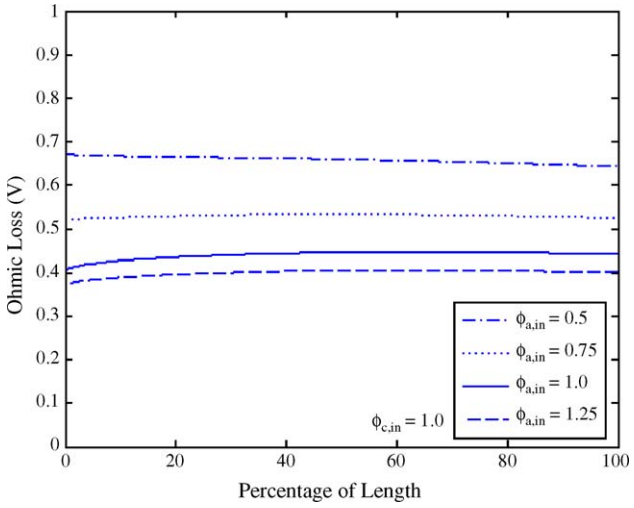

Fig. 9. Effect of anode inlet water content on the ohmic loss (pure oxygen; $\phi_{c,in} = 1.0$; $\phi_{a,in} = 0.5, 0.75, 1.0, 1.25$).

a higher membrane conductivity as shown in Figs. 2 and 3, which dominates the ohmic loss although the higher inlet water contents leads to higher current density in a certain area as shown in Figs. 4 and 6.

Fig. 11 shows the effect of anode inlet water content on the net water flux per proton. Near the inlet, the net water flux is higher due to high electro-osmotic drag coefficient near the anode inlet. The net water flux increase with anode inlet water content is because the higher anode water content provides higher electro-osmotic drag coefficient as shown in Fig. 12. The cathode inlet water content has almost no effect on the net water flux in this case as shown in Fig. 13.

Fig. 14 shows the effect of anode inlet water content on the partial pressure of hydrogen and oxygen along the channel. The higher the anode inlet water is, the lower the partial pressures are for both hydrogen and oxygen. For hydrogen, higher anode inlet water leads to higher partial pressure of

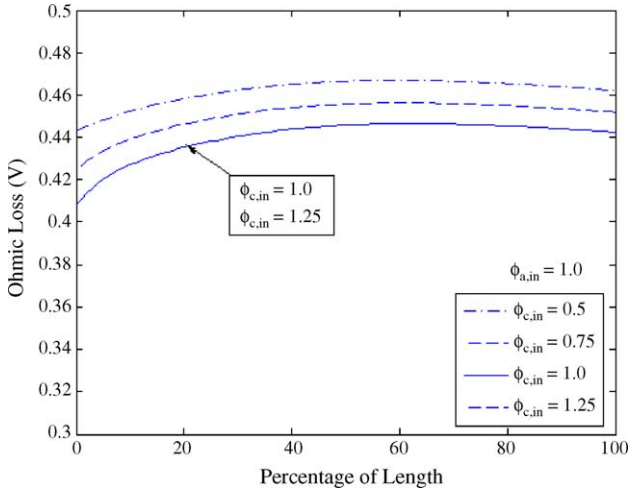

Fig. 10. Effect of cathode inlet water content on the ohmic loss (pure oxygen; $\phi_{a,in} = 1.0$; $\phi_{c,in} = 0.5, 0.75, 1.0, 1.25$).

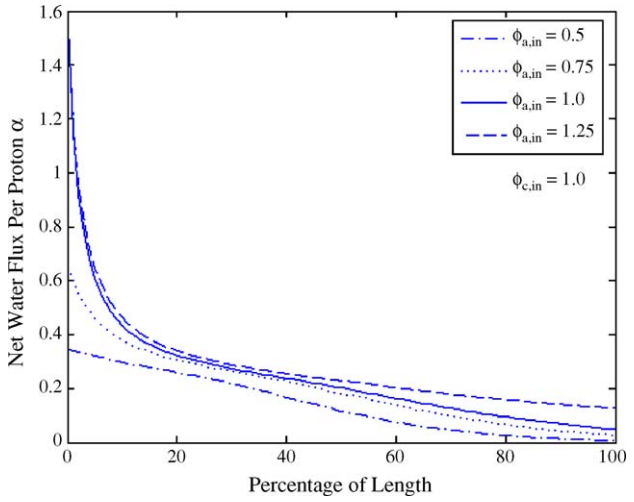

Fig. 11. Effect of anode inlet water content on net water flux per proton (pure oxygen; $\phi_{c,in} = 1.0$; $\phi_{a,in} = 0.5, 0.75, 1.0, 1.25$).

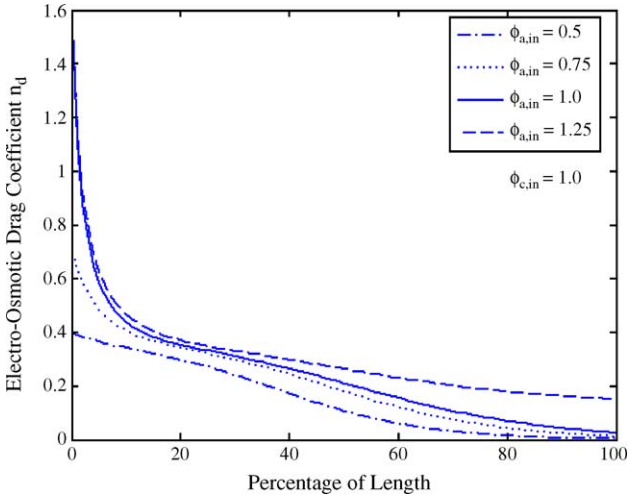

Fig. 12. Effect of anode inlet water content on electro-osmotic drag coefficient (pure oxygen; $\phi_{c,in} = 1.0$; $\phi_{a,in} = 0.5, 0.75, 1.0, 1.25$).

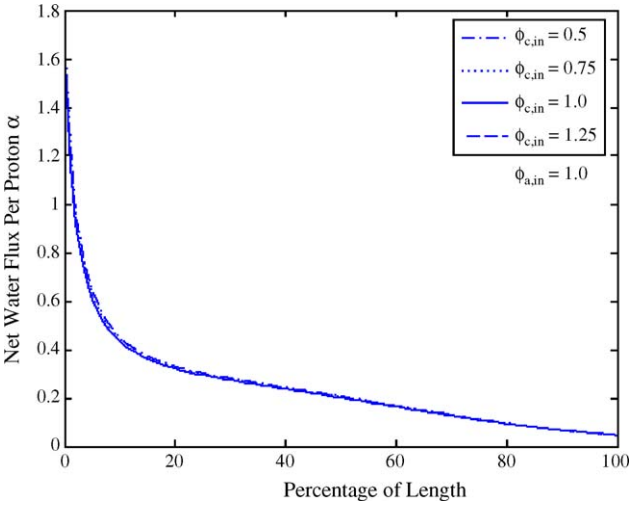

Fig. 13. Effect of cathode inlet water content on net water flux per proton (pure oxygen; $\phi_{a,in} = 1.0$; $\phi_{c,in} = 0.5, 0.75, 1.0, 1.25$).

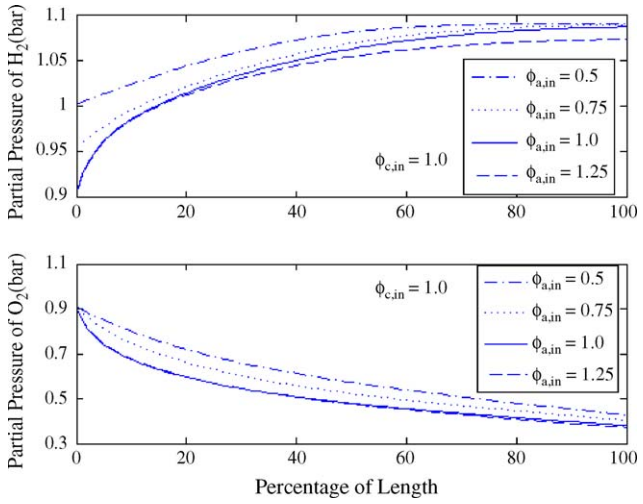

Fig. 14. Effect of anode inlet water content on the partial pressure of hydrogen and oxygen (pure oxygen; $\phi_{c,in} = 1.0$; $\phi_{a,in} = 0.5, 0.75, 1.0, 1.25$).

water vapor, which decreases the partial pressure of hydrogen. For oxygen, higher anode inlet water leads to higher water vapor transportation across the membrane that leads to lower oxygen partial pressure. Once the anode inlet has reached saturation condition, its effect on the partial pressure of oxygen is very small because the water vapor of anode side is enough for the requirement of transportation and the liquid water evaporates very slowly under this condition. Therefore, the increase of water vapor on anode side because of liquid water evaporation almost has no effect on the pressure of cathode side. Fig. 15 shows the cathode inlet water content on the partial pressure of oxygen and hydrogen. Increased cathode inlet water amount leads to lower partial pressure of oxygen before it attains saturation condition ($\phi_{c,in} = 1.0$). When $\phi_{c,in} > 1.0$, the liquid water does not have much effect on oxygen since the liquid water in cathode channel cannot evaporate to supplement water vapor in this case; because

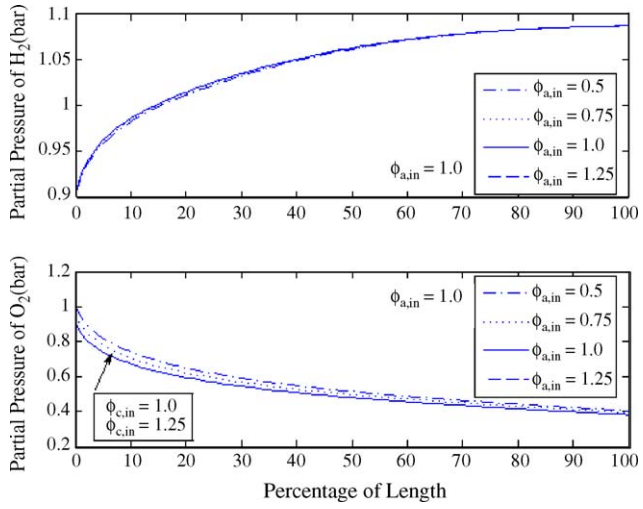

Fig. 15. Effect of cathode inlet water content on the partial pressure of hydrogen and oxygen (pure oxygen; $\phi_{a,in} = 1.0$; $\phi_{c,in} = 0.5, 0.75, 1.0, 1.25$).

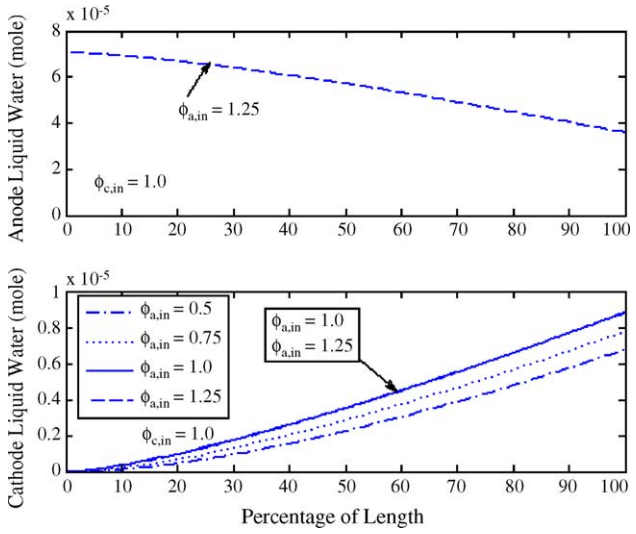

Fig. 16. Effect of anode inlet water content on the liquid water mole number (pure oxygen; $\phi_{c,in} = 1.0$; $\phi_{a,in} = 0.5, 0.75, 1.0, 1.25$).

the partial pressure of water vapor is greater than the saturation pressure. The effect of cathode inlet water on hydrogen partial pressure is very limited.

Fig. 16 shows the effect of anode inlet water content on the liquid water mole number. It is clear that there would be no liquid water in anode if the anode inlet water content is less or equal to one. When $\phi_{a,in} > 1.0$, in anode channel, the liquid water decreases along the channel since it evaporates to supplement vapor continuously. In cathode channel, the liquid water increases along the channel since vapor condenses to liquid due to more water supplied by the reaction. The increased anode inlet water amount corresponds to higher liquid water on the cathode side due to water transport across membrane from anode side to cathode side. Once the anode inlet reaches saturation, the liquid water has no such effect as shown in Fig. 16 for $\phi_{a,in} = 1.0$ and 1.25. As shown in Fig. 17,

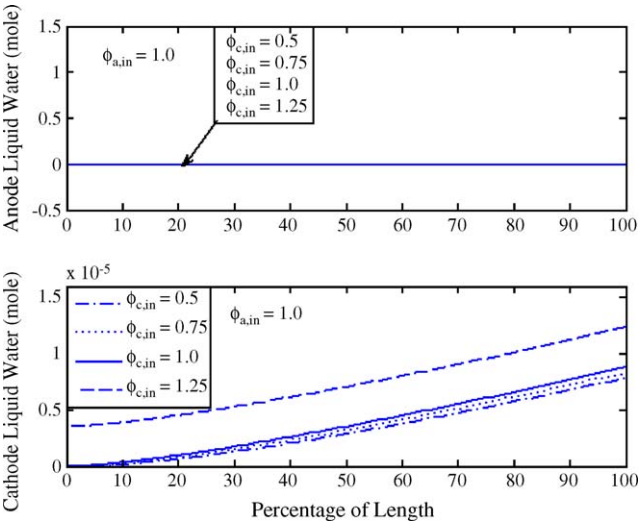

Fig. 17. Effect of cathode inlet water content on the liquid water mole number (pure oxygen; $\phi_{a,in} = 1.0$; $\phi_{c,in} = 0.5, 0.75, 1.0, 1.25$).

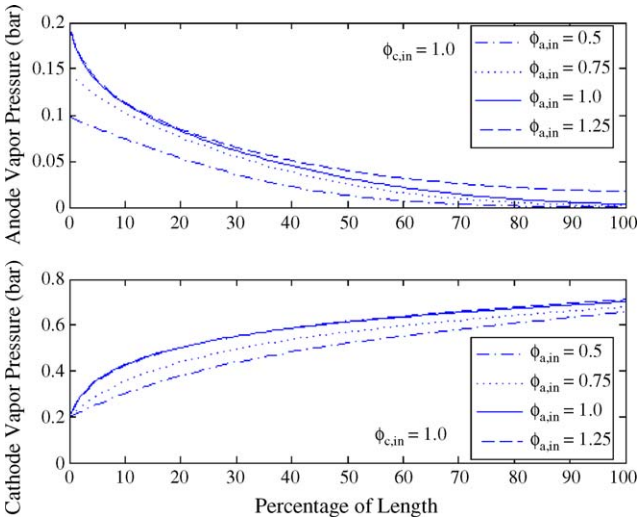

Fig. 18. Effect of anode inlet water content on the water vapor partial pressure (pure oxygen; $\phi_{c,in} = 1.0$; $\phi_{a,in} = 0.5, 0.75, 1.0, 1.25$).

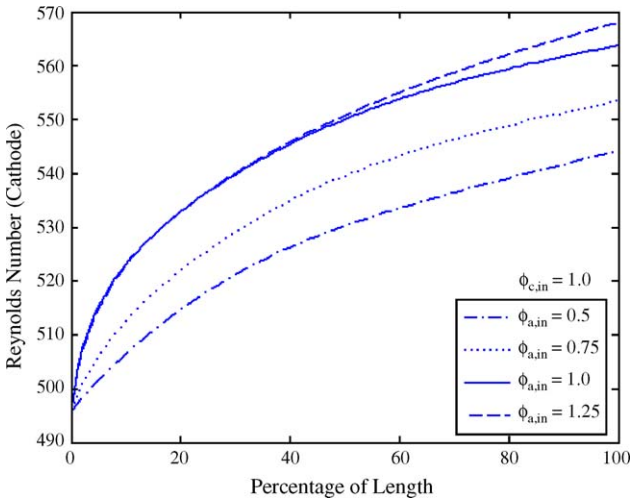

Fig. 20. Effect of anode inlet water content on the Reynolds number at cathode (air; $\phi_{c,in} = 1.0$; $\phi_{a,in} = 0.5, 0.75, 1.0, 1.25$).

higher cathode inlet water leads to higher liquid water in the cathode channels because more water vapor condensation occurs for the cases with higher cathode water content.

Fig. 18 shows the effect of anode inlet water content on the water vapor partial pressure along the channel. Vapor pressure decreases along the anode channel due to water transportation across the membrane from anode to cathode side. Vapor pressure increases along the cathode channel due to water transportation and electrochemical reaction. Increased anode inlet water content corresponds to increased vapor pressure for both sides. As shown in Fig. 19, the effect of cathode inlet water content on anode vapor pressure is relatively small since the effect of back diffusion and convection due to water vapor partial pressure difference between the anode and cathode is correspondingly small.

Reynolds number is one of the important parameters in fluid flow. Figs. 20 and 21 show the effects of anode and cathode inlet water content on the Reynolds number at the cathode along the channel. Reynolds number increases in the cathode because viscosity decreases, velocity increases and density does not change much along the channel as shown in the authors' previous study [17]. The bigger the inlet water content, the larger the velocity and Reynolds number at the cathode. For the present study, the flow is obviously in laminar flow regime. The Reynolds number in the cathode does not change when $\phi_{c,in} > 1.0$, this is because the liquid water volume is neglected in the present calculations.

The pressure loss cannot be neglected and it is one of the important parameters for fuel cell system design. Figs. 22 and 23 show the local pressure in the cathode along the channel. The local cathode pressure varies almost linearly. The bigger the inlet water amount, the larger the pressure

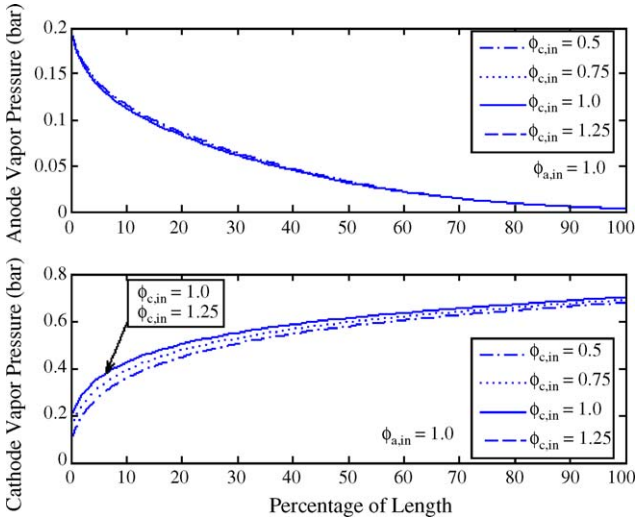

Fig. 19. Effect of cathode inlet water content on the water vapor partial pressure (pure oxygen; $\phi_{a,in} = 1.0$; $\phi_{c,in} = 0.5, 0.75, 1.0, 1.25$).

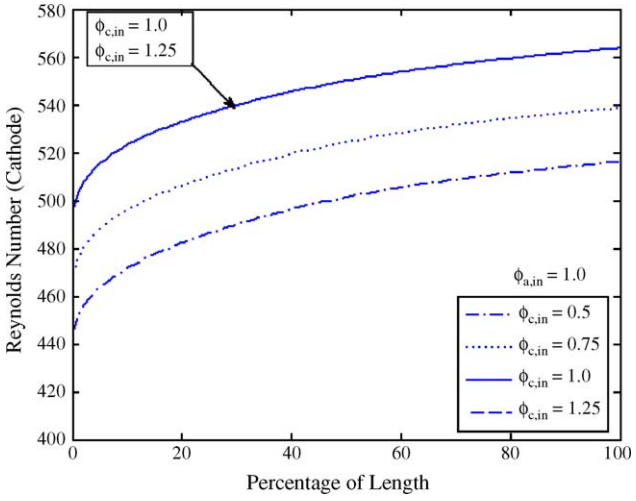

Fig. 21. Effect of cathode inlet water content on the Reynolds number at cathode (air; $\phi_{a,in} = 1.0$; $\phi_{c,in} = 0.5, 0.75, 1.0, 1.25$).

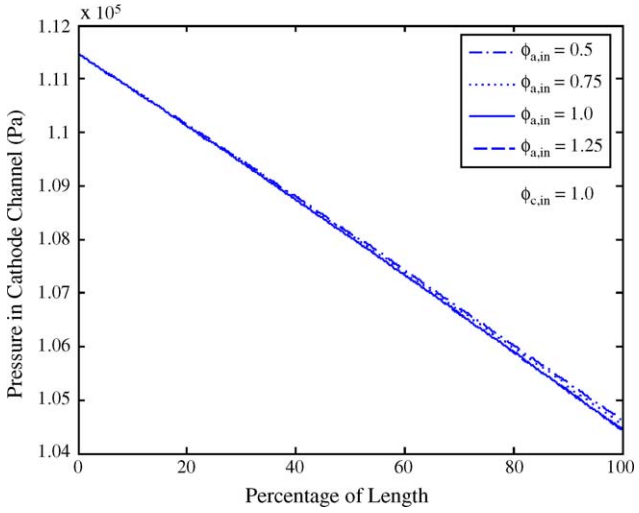

Fig. 22. Effect of anode inlet water content on the local pressure at cathode (air; $\phi_{c,in} = 1.0$; $\phi_{a,in} = 0.5, 0.75, 1.0, 1.25$).

drop. The pressure drop in the cathode is around 7000 Pa, which is very close to practical operating situation, e.g., the Nexa^{TM} Ballard PEM fuel cell operated at the authors' laboratory.

Pressure drop for different control volumes is not equal. The local pressure drop increases because volume flow rate increases. The required pumping power for the cathode increases with the increase of channel length, which is shown in Figs. 24 and 25. The greater the inlet water content at the anode and cathode, the larger the pumping power required. The total pumping power for cathode flow of a single cell is proportional to the number of channels (four channels for the present study).

Fig. 26 shows the effects of pressure loss in the flow channel and anode inlet water content on the power of a single fuel cell. It can also be seen that when the pressure loss is

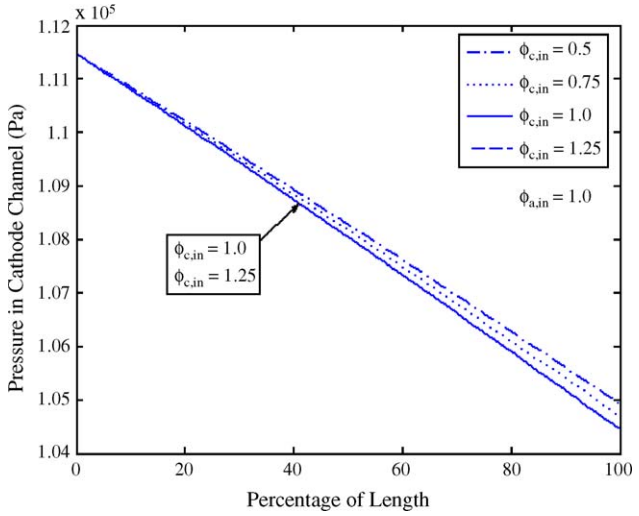

Fig. 23. Effect of cathode inlet water content on the local pressure at cathode (air; $\phi_{a,in} = 1.0$; $\phi_{c,in} = 0.5, 0.75, 1.0, 1.25$).

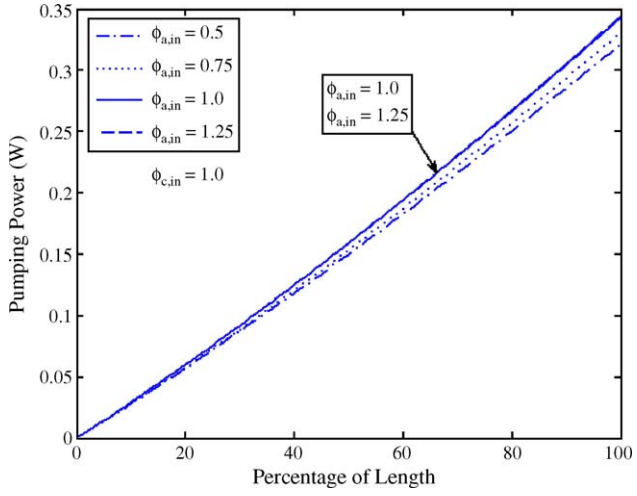

Fig. 24. Effect of anode inlet water content on the required pumping power for cathode (air; $\phi_{c,in} = 1.0$; $\phi_{a,in} = 0.5, 0.75, 1.0, 1.25$).

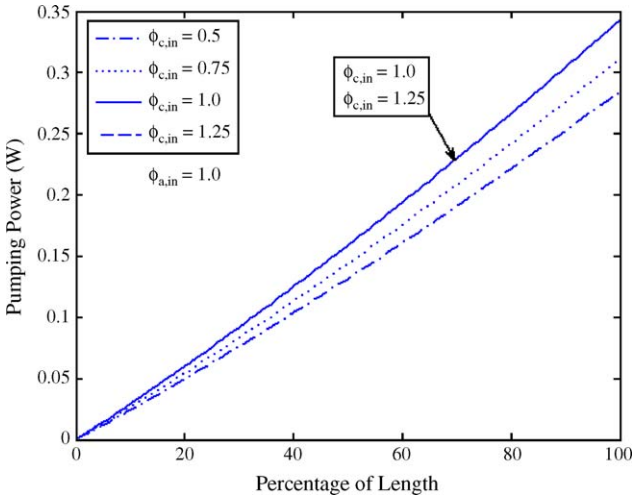

Fig. 25. Effect of cathode inlet water content on the required pumping power for cathode (air; $\phi_{a,in} = 1.0$; $\phi_{c,in} = 0.5, 0.75, 1.0, 1.25$).

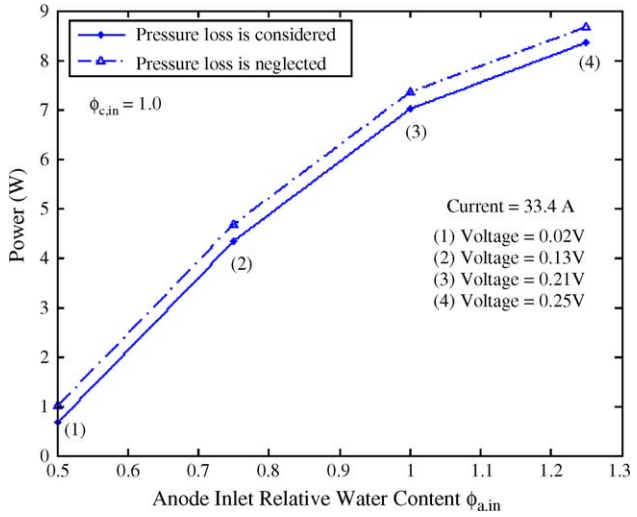

Fig. 26. Effects of anode inlet water content and pressure loss on the power of a single fuel cell (air).

Table 3
The effects of pressure loss and anode inlet water content on the power of the single cell

$\phi_{a,in}$	0.5	0.75	1.0	1.25
Voltage (V)	0.02	0.13	0.21	0.25
Current (A)	33.4	33.4	33.4	33.4
Power (W)	0.668	4.342	7.014	8.350
Power loss due to pressure loss (W)	0.334	0.334	0.334	0.334
Percentage of power loss due to pressure loss	50	7.7	4.8	4

considered, the cell power is lower than that without considering the pressure drop. The most important reason is that the pressure loss decreases the partial pressure of oxygen, which leads to higher activation loss. In addition, the pressure loss decreases the water content in the membrane, which decreases the membrane conductivity and increases the ohmic loss. In the case of a fixed average current density, the higher the anode inlet water content ($\phi_{a,in} = 0.5$–1.25), the higher the fuel cell power, i.e., the fuel cell performance can be improved by humidifying the anode. Further, injecting certain amount of liquid water into the anode inlet could improve the fuel cell output power. Table 3 gives detailed information of this effect. It can be seen that the percentage of power loss due to the pressure drop increases with the decrease of anode inlet water content. The lower the fuel cell power is, the higher this percentage would be.

5. Conclusions

The model for reacting fluids on both the air and hydrogen plates of a single PEM fuel cell, with water transport across membrane, water phase-change effect and pressure variation along the channel, has been developed and the predictions of this model can be used for the optimization of a PEM fuel cell. In addition, the effects of anode/cathode inlet relative water content on fuel cell performance were investigated. Based on this study, the following conclusions can be drawn:

1. The humidification of both anode and cathode sides are very important for the performance of PEM fuel cells.
2. The Water content of the anode side, which tends to dry-out, dominates membrane performance and plays a key role in the performance of PEM fuel cells.
3. Proper liquid water injection at the anode inlet could improve fuel cell performance since the liquid water could evaporate to generate water vapor and thus make the membrane hydrated.
4. Liquid water injection at the cathode inlet is not advocated since it would not improve the cell performance but increases the burden for water removal.
5. The pressure drop in the PEM fuel cell flow channels increases the pumping power cost. Therefore, particular attention must be paid to the pressure drop when designing a fuel cell, especially if air is used rather than pure oxygen. Pressure loss is one of the important parameters that affect total system efficiency and optimization.
6. When inlet humidification is applied to improve cell performance, the increase of pumping power and the burden of water removal because of humidification should also be considered in the system design.

Acknowledgement

This work was partially supported by AUTO21^{TM}—a Network of Centers of Excellence.

References

[1] P. Costamagna, S. Srinivasan, Quantum jumps in the PEMFC science and technology from the 1960s to the year 2000 Part II. Engineering, technology development and application aspects, J. Power Sources 102 (2001) 253–269.
[2] K. Yao, K. Karan, K. McAuley, P. Oosthuizen, B. Peppley, T. Xie, A review of mathematical models for hydrogen and direct methanol polymer electrolyte membrane fuel cells, Fuel Cells 4 (1–2) (2004) 3–29.
[3] D. Bernardi, M. Verbrugge, A mathematical model of the solid-polymer-electrolyte fuel cell, J. Electrochem. Soc. 139 (9) (1991) 2477–2491.
[4] D. Bernardi, M. Verbrugge, Mathematical model of a gas diffusion electrode bonded to a polymer electrolyte, AIChE J. 37 (8) (1991) 1151–1163.
[5] T.E. Springer, T.A. Zawodzinski, S. Gottesfeld, Polymer electrolyte fuel cell model, J. Electrochem. Soc. 138 (8) (1991) 2334–2342.
[6] T. Fuller, J. Newman, Water and thermal management in solid-polymer-electrolyte fuel cells, J. Electrochem Soc. 140(5) (1993) 1218–1225.
[7] T. Nguyen, R. White, A water and heat management model for proton-exchange-membrane fuel cells, J. Electrochem Soc. 140 (8) (1993) 2178–2186.
[8] J. Yi, T. Nguyen, An along the channel model for proton exchange membrane fuel cells, J. Electrochem. Soc. 145 (4) (1998) 1149–1159.
[9] R. Mosdale, S. Srinvasan, Analysis of performance and of water and thermal management in proton exchange membrane fuel cells, Electrochim. Acta 40 (4) (1994) 413–421.
[10] J.C. Amphlett, R.M. Baumert, R.F. Mann, B.A. Peppley, P.R. Roberge, Performance modeling of the Ballard Mark IV solid polymer electrolyte fuel cell, J. Electrochem. Soc. 142 (1) (1995) 1–8.
[11] C. Marr, X. Li, An engineering model of proton exchange membrane fuel cell performance, ARI 50 (1998) 190–200.
[12] K. Dannenberg, P. Ekdunge, G. Lindbergh, Mathematical model of the PEMFC, J. Appl. Electrochem. 30 (2000) 1377–1387.
[13] K. Hertwig, L. Martens, R. Karwoth, Mathematical modeling and simulation of polymer electrolyte membrane fuel cells, Fuel Cells 2 (2) (2002) 61–77.
[14] S. Ge, B. Yi, A mathematical model for PEMFC in different flow modes, J. Power Sources 124 (2003) 1–11.
[15] X. Xue, J. Tang, A. Smirnova, R. England, N. Sammes, System level lumped-parameter dynamic modeling of PEM fuel cell, J. Power Sources 133 (2004) 188–204.
[16] W. Pressure, S. Teukolsky, W. Vetterling, B. Flannery, Numerical Recipes in Fortran77—The Art of Scientific Computing, vol. 1, second ed., Cornell University, 1992, pp. 355–362.
[17] B. Zhou, Y. Zong, Relative humidity effects on the flow in PEM fuel cell cathode, CSME Forum (2004) 1063–1070.